

Modelling and Optimization of Oxalic Acid Removal by Layered Double Hydroxide

Sema Şentürk¹ , Halil Gamsızkan² , Mehmet Koray Gök^{1,3} , Yavuz Selim Aşçı⁴ , Aslı Gök^{1*} 

¹Department of Chemical Engineering, Istanbul University-Cerrahpasa, Istanbul/Türkiye.

²Department of Physics, Eskişehir Technical University, Eskişehir/Türkiye.

³Environmental and Earth Sciences Application and Research Center, Istanbul University-Cerrahpasa, Istanbul/Türkiye.

⁴Department of Chemistry, Istanbul University, Istanbul/Türkiye.

*aslig@iuc.edu.tr

Abstract

The main purpose of this study is the investigation of the optimization of the conditions of oxalic acid (OxA) adsorption using layered double hydroxide (LDH), modeling the adsorption with both an artificial neural network (ANN) and the response surface methodology (RSM). Mg-Al LDH, which was characterized by Fourier transform infrared spectroscopy (FTIR), X-ray diffraction (XRD) techniques and inductively coupled plasma mass spectrometry (ICP-MS), was synthesized via the co-precipitation method. The equilibrium time and kinetic model data required to realize the adsorption process design were examined. The process time, initial acid concentration, temperature, and adsorbent dosage as the independent variables were chosen while measuring the percentage of OxA removal. Modeling these results with both ANN and RSM techniques resulted in an ANN model showing a slightly better coefficient of determination than the RSM model. The models obtained in this study yielded consistent results for the optimum conditions of the process.

Keywords: Adsorption, Layered double hydroxide, Oxalic acid, Artificial neural network, Response surface methodology

Çift Tabakalı Hidroksit ile Oksalik Asit Uzaklaştırılmasının Modellenmesi ve Optimizasyonu

Özet

Bu çalışmanın temel amacı, oksalik asit (OxA) adsorpsiyon koşullarının çift tabakalı hidroksit (LDH) kullanılarak optimizasyonunun araştırılması, adsorpsiyonun hem tepki yüzeyi metodolojisi (RSM) hem de yapay sinir ağı (YSA) ile modellenmesidir. Mg-Al LDH, birlikte çöktürme yöntemiyle sentezlenmiş olup, fourier dönüşümlü kızılötesi spektroskopisi (FTIR), indüktif eşleşmiş plazma-kütle spektrometresi (ICP-MS) ve X-ışını kırınımı (XRD) teknikleriyle karakterize edilmiştir. Adsorpsiyon proses tasarımının gerçekleştirilmesi için gerekli olan denge süresi ve kinetik model verileri incelenmiştir. OxA uzaklaştırma yüzdesi ölçülürken bağımsız değişkenler olarak proses süresi, başlangıç asit konsantrasyonu, sıcaklık ve adsorban dozajı seçilmiştir. Bu sonuçların hem RSM hem de YSA teknikleriyle modellenmesi, RSM modelinden biraz daha iyi bir belirleme katsayısı gösteren bir YSA modeliyle sonuçlanmıştır. Modeller prosesin optimal koşulları için tutarlı sonuçlar vermiştir.

Anahtar Kelimeler: Adsorpsiyon, Çift tabakalı hidroksit, Oksalik asit, Yapay sinir ağı, tepki yüzeyi metodolojisi

1. INTRODUCTION

Oxalic acid (OxA), which ranks first among dicarboxylic acids, is commonly found in soil and water [1, 2]. It is also called ethanedioic acid and is abundantly found in many plants, such as spinach, rhubarb and lettuce [1, 3]. The industrial use of OxA as an agent or ligand includes the corncobs being simultaneously sweetened and fermented to produce ethanol, the depolymerization of lignocellulose to produce xylose from beechwood, and the adsorption of numerous heavy metals to increase the brightness and hardness of paper industry products. [2,4-5]. In addition, it is also used for photocatalytic activation [6, 7] and in the metalworking industry as a rust remover and a precipitating agent [8]. Apart from these, OxA is the exhaust by-product of automobiles. It can also contaminate the environment as a pollutant from all the processes mentioned above [9]. Considering the short-term side effects of OxA intake in humans and animals, it is very harmful due to the insoluble calcium salt that forms when combined with calcium and causes urinary stone formation. Stomach pain, vomiting, and coma may develop over time due to OxA buildup in the body. [10]. Many researchers seek more effective, cheaper and environmentally friendly methods to remove OxA from aqueous solutions. There are several methods to remove carboxylic acids from water. Calcium precipitation is the most common technique. However, it comes with the drawback of producing a lot of waste calcium and providing low yields. [11, 12]. Therefore, the researchers turned to find alternative separation methods. One of these methods is liquid extraction, which is advantageous regarding energy consumption. Kirsch and Maurer analyzed the liquid-liquid balance data of the aqueous solution of OxA using different organic solvents [13]. The other is the reactive extraction method, which has higher separation yields in aqueous solutions than physical extraction [14]. The third one is the membrane separation method, in which Manzak and Inal [8] examined the separation of OxA by Emulsion Type Liquid Membrane. Despite the fact that there are numerous ways to remove carboxylic acids from aqueous solutions [11], the adsorption methods are frequently preferred because of their low cost and ease of use [16, 17]. Jain et al. [18] used flayash, an adsorbent obtained as a waste product from thermal power plants, to remove OxA. Similarly, Singh et al. [19] examined the adsorption kinetics using an activated carbon-fly ash mixture to separate OxA.

Looking at studies on OxA removal in the literature, there is always a search for new materials to provide more economical and environmentally friendly separation adsorption properties and methods. In this regard, materials in the waste group, such as eggshells and commercial products such as A21 amberlist and activated carbon are used, as well as clay minerals such as hematite, montmorillonite, feldspar are also widely preferred [16,17,20-23]. Another type of adsorbent alternative to these materials is layered double hydroxide (LDH). It is an inorganic material, and the general formula for its chemical compositions is $[M^{II}_{1-x}M^{III}_x(OH)_2]^{x+} [A^{n-}_{x/n} \cdot yH_2O]^{x-}$ A^{n-} is an n-valent anion, M^{II} and M^{III} are divalent and trivalent metal cations, respectively. LDH, an anionic clay, is a useful, environmentally friendly adsorbent due to its ion exchange capacity [24-25]. Gök et al. [26] used this adsorbent to remove malic acid from an aqueous solution and investigated the kinetics. Hosseini and Akbari [27] used ZnO-Mg/Al LDH as an adsorbent-photocatalyst to remove the dye pollutants, modeled by RSM and ANN. Similarly, Yasin et al. [28] used tartrate-Mg-Al LDH to remove lead ions by optimization with a hybrid ANN-genetic algorithm.

One of the most important reasons LDH has used such an active adsorbent in the literature is that it is a host-guest material. Because of this, we evaluated LDH adsorption for the first time in this study to remove OxA from aqueous solutions. By analyzing the effects of temperature, process time, initial acid concentration, and adsorbent dose on the adsorption process, as well as by modeling the data using the response surface approach and an ANN, the process was analyzed and optimized. The response surface methodology (RSM) is a statistical approach for process optimization where multiple independent input factors influence a dependent output variable. The response is the output variable. When forecasting an outcome, RSM, as an improved systematic method to experimentation, concurrently takes into account every aspect of the process. One of its key benefits is that it just requires a small number of experimental runs to identify the ideal experimental settings. A mathematical model known as an artificial neural

network (ANN) simulates how biological neural networks work while processing information. Input and output layers are typically joined by one or more hidden layers; the number of those layers depends on the nature of the experiment. A neural network's ability to perform some internal calculations while using a set of input values to determine output is its key characteristic. Using these models, we deduce optimal reaction points and comment on the importance of the independent process variables.

2. MATERIALS AND METHODS

2.1 Materials

The following items were acquired from Sigma (USA): OxA, sodium hydroxide, Magnesium chloride hexahydrate ($\text{MgCl}_2 \cdot 6\text{H}_2\text{O}$), and Aluminum chloride hexahydrate ($\text{AlCl}_3 \cdot 6\text{H}_2\text{O}$). Without additional purification, all compounds were used.

2.2 Synthesis and Characterization of Mg-Al-LDH

2.2.1 Synthesis

The chloride form of Mg-Al LDH adsorbent ($\text{MgCl}_2 \cdot 6\text{H}_2\text{O}:\text{AlCl}_3 \cdot 6\text{H}_2\text{O} - 3:1$ mmol) was synthesized by standard co-precipitation method under a nitrogen environment at ambient temperature. [26]. Briefly, 10 mL of decarbonated water was used to dissolve the magnesium and aluminum salts. The salt solution was then promptly poured into a 40 mL solution of 6 mmol NaOH while constantly agitated for 10 minutes. After aging for one hour under a nitrogen atmosphere, the resultant slurry was centrifuged twice for 5 minutes at 4500 min^{-1} rpm and against at 6000 min^{-1} rpm for 10 min one time, washing with water before each centrifugation process. The precipitate was lyophilized at 0.01 mbar pressure at $-55 \pm 1 \text{ }^\circ\text{C}$ (Lyoquest, Telstar, Spain).

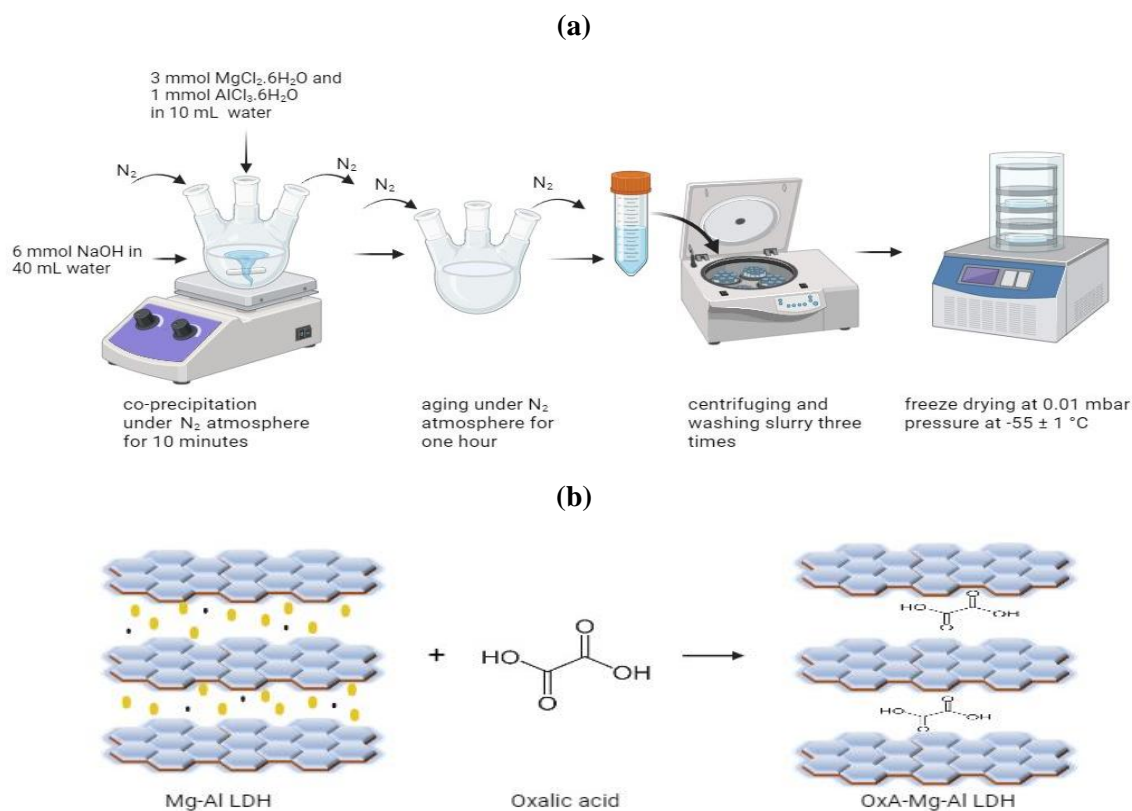


Figure 1. Schematic diagram of (a) synthesis of Mg-Al LDH adsorbent and (b) intercalation of oxalic acid into Mg-Al LDH

2.2.2 Characterization

OxA, Mg-Al LDH and OxA-Mg-Al LDH were characterized with FTIR technique (Cary 630, Agilent; USA). Their FTIR spectra were taken using KBR disks (sample: KBR; 1:200 w/w) over 4000-650 cm^{-1} , and X-Ray Powder Diffractometer with Cu K radiation ($\lambda = 1.5406 \text{ nm}$) was used to analyze their crystalline structures (Rigaku D/Max-2200/PC; Japan) at 30 mA and 40 kV ($1^\circ/\text{min}$; $2\theta = 5^\circ - 30^\circ$). ICP-MS analyze was used to determine the weight % ratio of Mg and Al (Thermo Scientific Element X-SERIES 2 (USA)).

2.3 Adsorption Experiments and Experimental Design

Our purpose for applying experimental design is to determine the optimum process point, which can be a minimum or a maximum, depending on the desired response. The optimum point reduces the time and the cost of the process and is used by process engineers to design an economical process [29]. With the trial version of Design-Expert 11, the experimental design for this investigation was carried out. Central Composite Design (CCD) was selected for the adsorption studies. A general quadratic equation, denoted as Eq. 1, was employed as the study's model.

$$y = \beta_0 + \sum_{j=1}^k \beta_j x_j + \sum_{j=1}^k \beta_{jj} x_j^2 + \sum \sum_{i < j} \beta_{ij} x_i x_j + \epsilon \quad (1)$$

A simplified equation form can define the process values after a detailed ANOVA analysis of the experimental data [30]. A total of 54 experimental points to apply both ANN and RSM methodologies were investigated. Time (X_1), starting acid concentration (X_2), adsorbent quantity (X_3), and temperature (X_4) were chosen as the independent variables for the experimental design. The recovery percentage of OxA was the dependent output (Y). α value is the distance between the experimental point and the design center point, which was chosen as 1. Coded variables with their corresponding levels are given in Table 1.

Stock acid solutions were prepared with distilled water according to the experimental design points. First, 5 mL of acid solution was combined with the adsorbent. The flask was then covered with a glass tap, set into a thermostat-controlled water bath, and shaken continuously at 120 rpm (Nüve Shaker ST30). After the necessary amount of time had passed for adsorption, LDH was removed from the acid solution using a 0.20 m RC Syringe filter, and the sample was centrifuged for 10 minutes at 9000 rpm. Acid-base titration measured the OxA concentration (Schott Titroline Easy module 2; Germany).

Table 1. Experimental design coded variables

Coded Factor Level	-1	0	1
Time (min) (X_1)	2	6	10
Initial Acid Concentration (% w/w) (X_2)	3	5	7
Adsorbent amount (g) (X_3)	0.05	0.25	0.45
Temperature (K)(X_4)	298	308	318

The Recovery (R) formula is as follows,

$$R (\%) = \frac{C_0 - C_e}{C_0} \times 100 \quad (2)$$

where the initial and final acid concentrations are C_0 and C_e (mg/L), respectively. Q_e (mg/g) was calculated according to the formula below, where V (L) is the volume of the solution used, and m is the adsorbent amount as g.

$$Q_e = (C_0 - C_e) \frac{V}{m} \quad (3)$$

For the equilibrium experiments, solutions of OxA at 3, 4, 5, 6, 7 and 8 (w/w %) concentrations were prepared with distilled water. These acid solutions were treated at 298, 308, and 318 K with 0.1 g LDH in

a temperature-controlled shaker water bath (Nüve Shaker ST30) until the equilibrium concentration was reached. For the kinetic experiments, 5% OxA solution was mixed with 0.1 g of LDH for up to 10 min at 298 K. The final acid concentration was determined by volumetric titration. All experiments were repeated three times ($n=3$).

2.4 Artificial Neural Network Modeling

Modeling the N -dimensional response surface using a feed-forward ANN has also been performed. A neural network is a mathematical construct loosely inspired by biological neural networks in animal brains. An ANN in the context of this study consists of interconnected “neurons”; each neuron sums its weighted input values, adds a scalar called bias, uses the result as the argument of a so-called transfer function and passes along this function value to the neurons it’s connected. Therefore, the output of an individual neuron is determined as:

$$y = f(b + \sum_i W_i x_i) \quad (4)$$

where x_i are input values, W_i are connection weights, b the bias term and f the transfer function. In an ANN, neurons are organized in layers, and they are only connected to the neurons at an adjacent layer. A layer of neurons that are only connected to another layer is called a hidden layer (Figure 2). The user defines characteristic parameters of an ANN such as the network topology and the activation functions. A neural network is trained with a set of input-output data. The training procedure aims to adjust connection weights and biases, so the network produces outputs closest to the ones corresponding to a given set of inputs. A well-designed and trained ANN can generalize and yield good results for inputs other than the values it’s trained with.

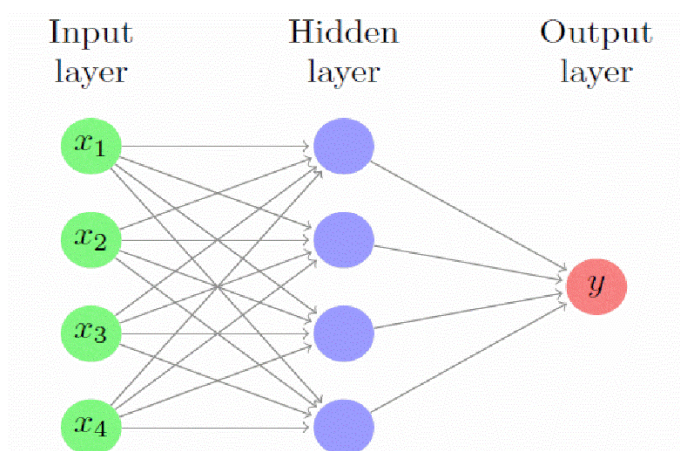


Figure 2. Topology of the ANN model used in this study. x_i are the input features, while y is the target variable.

3. RESULTS AND DISCUSSION

The synthesis of Mg-Al LDH for OxA adsorption was carried out by the co-precipitation method. Salts-enriched species precipitate in this method based on the pH of the slurry. [31]. The pH of the slurry was kept at 8.3 to obtain the Al-enriched layered content of LDH. The molecular formula of Mg-Al LDH is $[\text{Mg}_{0.65}\text{Al}_{0.35}(\text{OH})_2](\text{Cl})_{0.35} \cdot 0.58\text{H}_2\text{O}$, and the atomic ratio (Mg/Al) is 1.88.

3.1 Fourier Transform Infrared Spectroscopy

The FTIR spectra of the OxA, Mg-Al LDH and OxA-Mg-Al LDH are given in Figure 3. The broadband due to the OH stretching vibrations of COOH groups at $3300\text{-}3550\text{ cm}^{-1}$ region (max at 3432 cm^{-1}), the sharp absorption band related to the stretching vibrations of C=O bonds in COOH groups at max. 1696

cm^{-1} and the sharp absorption band related to the OH deformation vibrations of COOH groups at the $1380\text{-}1250\text{ cm}^{-1}$ region (max. 1256 cm^{-1}) were seen in the FTIR spectrum of OxA.

The broadband due to the asymmetric and symmetric stretching vibrations of hydroxyl groups in the LDH layers (Mg-Al-OH) and at $3350\text{-}3700\text{ cm}^{-1}$ region (max at 3548 cm^{-1}) was seen in FTIR spectra of Mg-Al LDH. Moreover, the weak broadband due to the deformation bending vibrations of water between these layers max at 1630 cm^{-1} was also seen. However, a small sharp band is caused by the asymmetric stretching vibration of the CO_3^{2-} , which occurs in a minor quantity during the synthesis of LDH under a nitrogen atmosphere to prevent excess carbonate contamination (at max. 1360 cm^{-1}).

FTIR analysis was used to study the overall changes in the structure of Mg-Al LDH caused by OxA adsorption. As seen in FTIR spectra of OxA-Mg-Al LDH, the broadband due to the stretching vibrations of OH groups has shifted to the max at 3448 cm^{-1} . Moreover, the absorption bands or shoulders that appeared at approximately $1710\text{-}1630\text{ cm}^{-1}$ region (max at 1697 cm^{-1} and 1638 cm^{-1}) were attributed to stretching vibrations of C=O bonds and deformation bending vibrations of the water molecule. The weak absorption bands that appeared at approximately $1450\text{-}1300\text{ cm}^{-1}$ region (max at 1407 , 1375 and 1328 cm^{-1}) were related to a combination band that stretched vibrations of C=O bonds and deformation vibrations of OH groups [32].

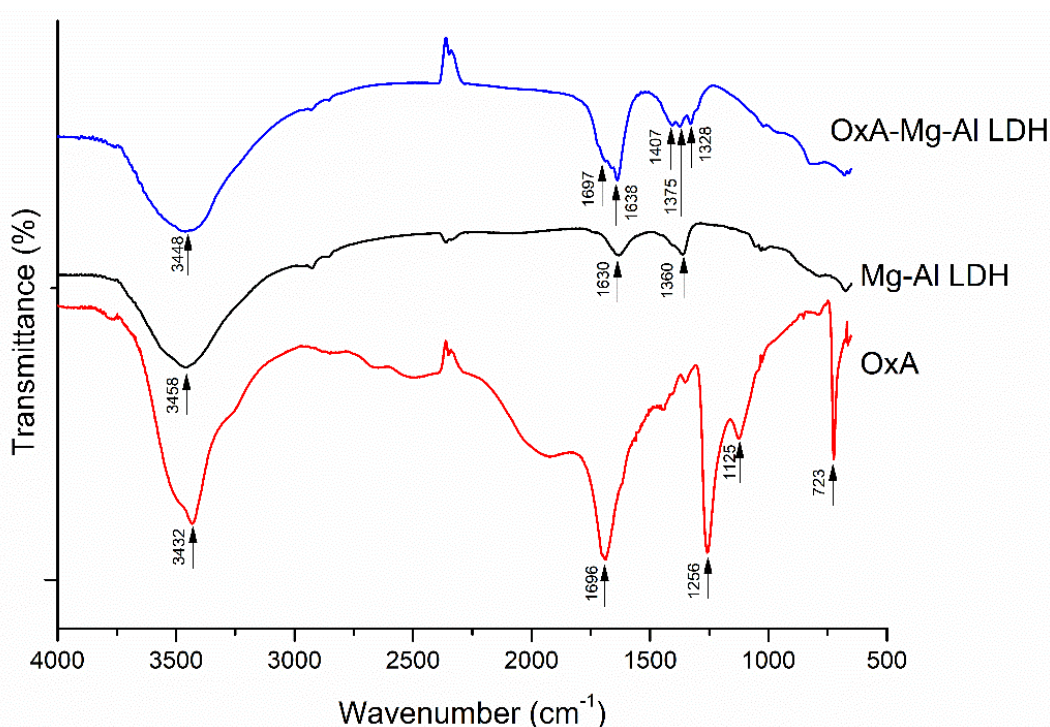


Figure 3. FTIR spectra of Mg-Al LDH and OxA-Mg-Al LDH

3.2 XRD

Powder XRD (PXRD) patterns of Mg-Al LDH and OxA-Mg-Al LDH were compared to study the OxA adsorption onto Mg-Al LDH. Figure 3 shows the results for Mg-Al LDH and OxA-Mg-Al LDH. In the PXRD pattern of Mg-Al LDH, the main strong peak (003) around $2\theta=11.3^\circ$ corresponding to $d=0.7778\text{ nm}$ gives information about the basal spacings of two consecutive brucite-like hydroxide layers. According to this, in the PXRD pattern of OxA-Mg-Al LDH, the main strong peak in Mg-Al LDH shifted to around $2\theta=8.8^\circ$ corresponding to $d=1.003\text{ nm}$ by the reduction of the intensity of d003 in LDH. The basal spacing of LDH expands from 0.7778 to 1.003 nm after the adsorption of OxA onto LDH, resulting from ion exchange between chloride (partially carbonate) ions and OxA in interlayer spaces (Figure 1.(b)).

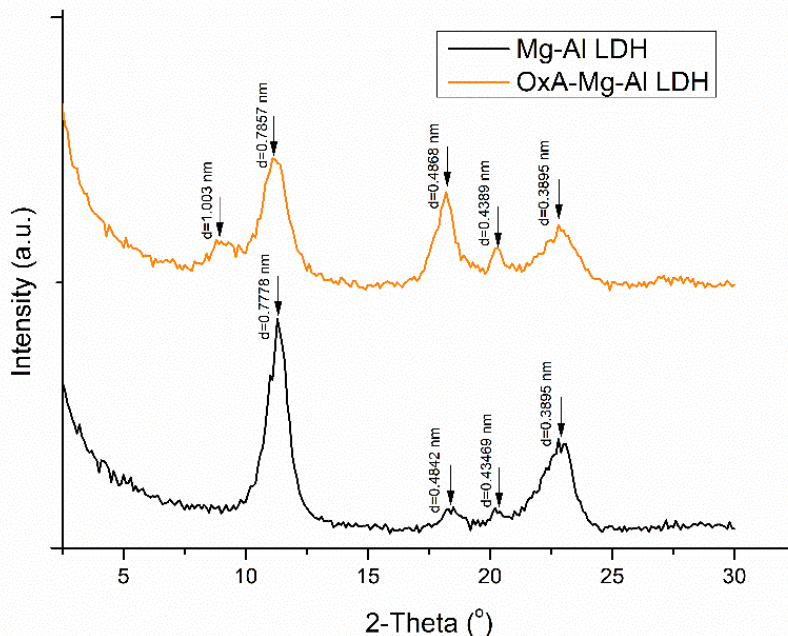


Figure 4. PXRD patterns of Mg-Al LDH and OxA-Mg-Al LDH

3.3 Equilibrium and Kinetic Adsorption Models

Experimental studies were conducted to determine the equilibrium time of the adsorption process and kinetic model. For this purpose, the compatibility of the adsorption kinetics with the Elovich equation, the Lagergren rate equation and the Pseudo-second-order models were investigated. The equations of these three models are given in Table 2 [33-35]. Once evaluated, the results obtained with these three model equations were highly compatible. However, when the theoretical and experimental results were compared, it was found that the best equation that models the adsorption kinetics of OxA on LDH was the Lagergren rate equation, also known as the false first order. The obtained R2 values and the equation parameter values are shown in Table 2.

Table 2. Kinetic parameters for the adsorption of OxA by LDH

Elovich Equation	α	β	R^2
$Q_t = \frac{1}{\beta} \ln(\alpha \cdot \beta) + \frac{1}{\beta} \ln(t)$	4.36	0,78	0.9901
Lagergren rate equation	Q_e	K_1	R^2
$\log(Q_e - Q_t) = \log Q_0 - \frac{k_1}{2.303} t$	7.53	0.16	0.9991
Pseudo second order	Q_e	K_2	R^2
$\frac{t}{Q_t} = \frac{1}{k_2 Q_e^2} + \frac{1}{Q_e} t$	76.41	0.027	0.9897

Adsorption isotherms assist us in understanding adsorption mechanisms and developing innovative industrial processes. The isotherms of Langmuir, Freundlich, and Temkin were explored using acid-starting solutions at various temperatures. The linearized equations (Table 3) are used to examine the adaptation of the isotherms [36]. It was observed that high compliance was achieved for all isotherms. However, it can be said that the Langmuir isotherm provides the best fit between the adsorption isotherms. The obtained values of R2 and isotherms are given in Table 3.

Table 3. Isotherm constants adsorption of OxA onto LDH

	T / K	Q ₀ /mg·g ⁻¹	K _L /g·L ⁻¹	R ²
Langmuir Isotherm $\frac{C_e}{Q_e} = \frac{1}{K_L Q_0} + \frac{C_e}{Q_0}$	298	573	9.54	0.9992
	308	681	12.33	0.9987
	318	742	15.12	0.9983
	T / K	n	K _f	R ²
Freundlich Isotherm $\log Q_e = \log K_f + (1/n)\log C_e$	298	1.97	0.41	0.9929
	308	1.31	0.68	0.9790
	318	0.95	0.97	0.9951
	T / K	B ₁	K _T	R ²
Temkin Isotherm $Q_e = B_1 \ln(K_T) + B_1 \ln(C_e)$	298	15.87	0.71	0.9974
	308	17.15	0.93	0.9895
	318	20.25	1.25	0.9916

The thermodynamic properties of an adsorption process can change under the influence of many parameters. Although it is very difficult to analyze them, some parameters can be used for some basic interpretations. The most important ones are standard free energy (ΔG°), enthalpy (ΔH°) and entropy (ΔS°). ΔG° is determined by using the following equation;

$$\Delta G^\circ = -RT \ln(K) \quad (5)$$

Where R is the universal gas constant, T is temperature, and K is the Langmuir constant. Van't Hoff equation is utilized to determine the values of (ΔH°) and (ΔS°):

$$\ln(K) = -\frac{\Delta H}{RT} + \frac{\Delta S}{R} \quad (6)$$

ΔH and ΔS were calculated from the slope and the intercept of the line in the graph of $\ln(K)$ versus $1/T$, respectively. Comments that can be made through these parameters are; The positive or negative value of ΔG° indicates the spontaneous realization of the adsorption without an external effect. Adsorption occurs negatively for negative values. Negative values of ΔH° adsorption are indicative of the fact that the adsorption is physical and exothermic. The results obtained from our studies are presented in Table 4.

Table 4. Thermodynamic parameters for the adsorption of OxA by LDH

T / K	(ΔG°) (kJ . mol ⁻¹)	(ΔH°) (J . mol ⁻¹)	(ΔS°) (J . mol ⁻¹ . K ⁻¹)
298	-6.85	- 17.72	59.28
308	-9.97		
318	-13.64		

Overall, when comparing our findings to those of earlier research, Dilek et al. employed Amberlyst A21 as an adsorbent to oxalic acid. Recovery of acid value is 27 % for 5% acid concentration. Ozcan et al., performed an adsorption with multiwalled carbon nanotubes this investigation results were similar to previous study. Our outcomes shows that LDH is an effective and environmentally friendly adsorbent for oxalic acid adsorption.

3.4 RSM Modeling and Optimization

In order to evaluate the effect of each factor on the response, one-way analysis of variance (ANOVA) was applied to experimental data and the results are given in Table 5. The model F value is found to be 53.28, which means that the model is significant. If $p < 0.05$ indicates significance, the relevant model terms are determined to be X_1 , X_2 , X_3 , X_1^2 , X_3^2 and X_4^2 . The final equation in terms of the coded factors is given below;

$$Y = +45.21 + 4.61 X_1 - 2.65 X_2 + 22.12 X_3 - 6.56 X_1^2 - 11.45 X_3^2 + 8.38 X_4^2 \quad (7)$$

ANOVA gives a lack of fit value of 22.55, which is significant. Although a significant lack of fit values are undesirable, it is usually the result of replicate run results of independent variables as very close or exactly the same [37,38]. The predicted regression coefficient (R^2) was 0.9064, and the adjusted R^2 value calculated with Design-Expert software was 0.9325. The fact that both coefficients are close to each other indicates the suitability of this model. R^2 value was also 0.9503. Adequate precision (AP) terms stand for the signal-to-noise ratio. It should be greater than 4 for an adequate signal, calculated as 22.494. Therefore, this model can be used to navigate the design space.

Table 5. ANOVA test for OxA Adsorption

Source	Sum of Squares	Df	Mean Square	F	P-Value
Model	20736.58	14	1481.18	53.28	<0.0001
X_1	765.65	1	765.65	27.54	<0.0001
X_2	313.21	1	313.21	11.27	0.0018
X_3	17662.03	1	17622.03	633.87	<0.0001
X_4	88.60	1	88.60	3.19	0.0820
X_1X_2	45.34	1	45.34	1.63	0.2091
X_1X_3	46.29	1	46.29	1.67	0.2045
X_1X_4	16.33	1	16.33	0.59	0.4480
X_2X_3	32.49	1	32.49	1.17	0.2863
X_2X_4	29.93	1	29.93	1.08	0.3058
X_3X_4	5.94	1	5.94	0.21	0.6464
X_1^2	221.07	1	221.07	7.95	0.0075
X_2^2	0.59	1	0.59	0.0021	0.8852
X_3^2	673.82	1	673.82	24.24	<0.0001
X_4^2	361.47	1	361.47	13	0.0009
Residual	1084.23	39	27.80		
Lack Of Fit	960.67	10	96.07	22.55	<0.0001
Pure Error	123.57	29	4.26		
Cor Total	21820.82	53			
Sd =5.27 $R^2=0.9503$ $R^2_{(Adj)}=0.9325$ $R^2_{(Pred)}=0.9064$ %CV=13.67 AP=22.494					

The quadratic model's 3D surface graphs were drawn by holding two parameters constant for each time (Figure 5). As seen from Figures 4a, 4b and 4d, the most effective parameter of the model is the amount of adsorbent. Figure 5a shows the effect of the amount of adsorbent and the initial acid concentration on removing OxA from water. In order to observe only the change in the adsorbent amount, the other parameters were fixed ($X_1 = 6$ min; $X_2 = 3\%$; $X_4 = 308K$). Thus, while the amount of adsorbent increases from 0.05g to 0.45g, the removal percentage (%) also increases from 15.2% to 57.4%.

Although the initial acid concentration has a lesser effect than the amount of adsorbent, it reduces the removal with increasing concentration. For example, when the parameters are fixed to $X_3=0.45\text{g}$, $X_1=6$ min, $X_4=308\text{K}$, while initial acid concentration increases from 3% to 7%, the removal percentage decreases from %57.4 to %53. This effect could also be observed in Figures 4c and 4e. Figures 4c and 4f show that the removal percentage increases with time. For example, when the parameters were fixed to $X_2=5\%$, $X_3=0.25$ g, $X_4=298\text{K}$, the removal percentage increases with increasing time (10 min) from 44.7% to 52.4%. Finally, as seen in Figures 4e and 4f, the effect of temperature on the adsorption process reduces the removal percentage. For example, when the parameters were fixed to $X_1=6$ minutes, $X_2=5\%$, $X_3=0.45$ g, the removal percentage decreases with rising temperature (from 298 K to 318 K) from 66.26% to 62.2%.

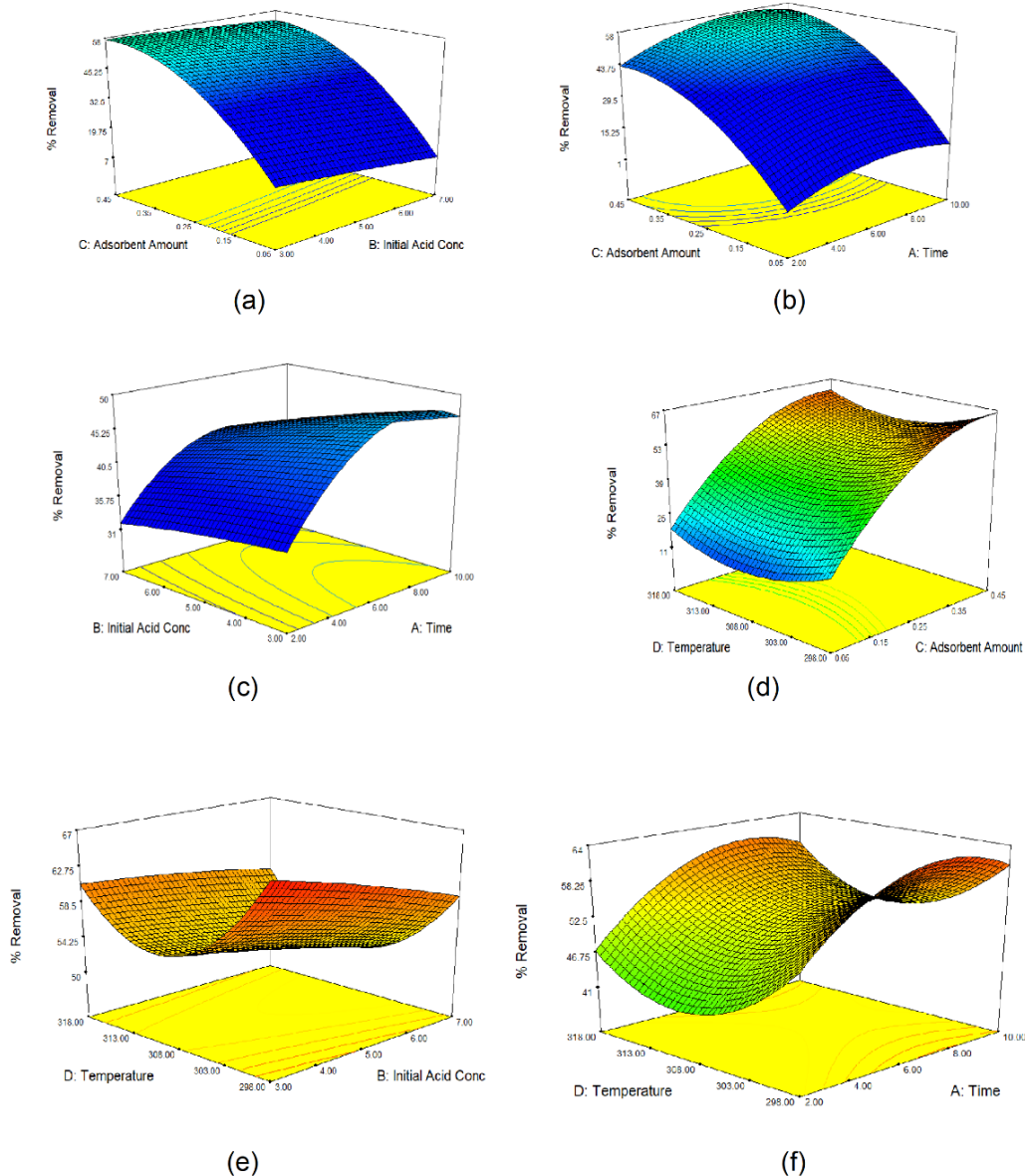


Figure 5. Response surface of removal (%) of OxA from water as a function of (a) adsorbent amount (g) and initial acid concentration (w/w %); (b) adsorbent amount (g) and time (min); (c) initial acid concentration (w/w %) and time (min); (d) temperature ($^{\circ}\text{K}$) and adsorbent amount (g); (e) temperature ($^{\circ}\text{K}$) and initial acid concentration (w/w %); (f) temperature ($^{\circ}\text{K}$) and time (min).

3.5 Artificial Neural Network Modeling

Practical applications of RSM and ANN methods include determining the response's best value, determining enhanced or ideal process settings, and identifying process weaknesses. If the process variables are complicated, it is crucial to construct and adapt intricate experimental protocols utilizing the design of experiments (DOE) method in conjunction with various modeling and optimization tools like RSM and ANN in order to obtain accurate data. For this purpose, after RSM, we applied ANN to the experimental data. ANN libraries provided by the scikit-learn package were used. The input features we used with our model are the reaction time, initial acid concentration, adsorbent amount and temperature. Our target variable was percent removal. We measured ANN regression performance with two commonly used statistics. First is the mean squared error (MSE), defined as:

$$MSE = \frac{1}{N} \sum_{i=1}^{i=N} (y_{i,pred} - y_{i,data})^2 \tag{8}$$

where y is the target variable in a sample of N measurements. Second performance statistic we used is the coefficient of determination (R^2), defined as:

$$R^2 = 1 - \frac{\sum_{i=1}^{i=N} (y_{i,pred} - y_{i,data})^2}{\sum_{i=1}^{i=N} (y_{i,pred} - \bar{y}_{data})^2} \tag{9}$$

where \bar{y}_{data} is the mean of target variable data:

$$\bar{y}_{data} = \frac{1}{N} \sum_{i=1}^{i=N} y_{i,data} \tag{10}$$

We trained the ANN with 80% of available experimental data chosen randomly, and the remaining data were used as the test sample. Training data was used to train the ANN, while test data was used to assess that the model was not overfit. The ANN itself must start training with a set of initial weight and bias values and as is the common practice these values were chosen randomly. Since ANN model performance is sensitive to feature ranges, feature scaling is an important part of ANN data preprocessing. We tested two feature scaling algorithms; the “standard” and the “min-max” algorithms. The standard algorithm scales the input features, so their distributions have zero mean and unit variance. On the other hand, min-max scaler scales the features, so their values lie in a user-defined range. Our performance results for different scaling choices can be seen in Table 6. Although the observed performances are similar, the standard scaler shows slightly better performance, so we utilized this normalization method in this study.

Table 6. Comparison of the effects of different normalizations method on model performance with an ANN having a topology of 4:4:1.

Scaler	Train set		Test set	
	MSE	R^2	MSE	R^2
Standard	2.08	0.996	16.74	0.966
Min-max [0, 1]	2.65	0.994	16.92	0.965
Min-max [-1, 1]	2.10	0.996	16.96	0.965

For the model topology, we used a single hidden layer network. We tested the modeling performance of models with different numbers of hidden layer neurons. The results are shown in Table 7 for comparison. Here we observe that topologies with 3 and 4 hidden layer neurons yield the best regression performance. This should be expected considering the size of our dataset. Considering the model performance on both training and test datasets, also the number of free parameters each topology requires, we chose 4:4:1 as the optimal topology for this study.

Table 7. Comparison of model performance versus network topology

ANN topology	Train set		Test set	
	MSE	R^2	MSE	R^2
4:2:1	16.74	0.965	29.82	0.939
4:3:1	8.65	0.982	21.73	0.955
4:4:1	2.08	0.996	16.74	0.966
4:5:1	1.45	0.997	20.51	0.958
4:6:1	2.06	0.996	16.21	0.967

About the transfer functions, we considered three options: ReLU, logistic and tanh. Among these, logistic and tanh are sigmoid type (s-shaped) nonlinear functions where the logistic function is defined as $f(x) = 1/(1 + e^{-x})$. ReLU is a “nonlinearized” identity function with a rather simple form: $ReLU(x) = \max(0, x)$. Model performances for different transfer functions are shown in Table 8. In this study, we chose the logistic function as the transfer function as it yielded the best performance.

Table 8. Comparison of the effect of transfer function on model performance with an ANN having a topology of 4:4:1.

Transfer function:	Train set		Test set	
	MSE	R^2	MSE	R^2
tanh	6.17	0.987	36.79	0.925
logistic	2.08	0.996	16.74	0.966
ReLU	27.54	0.942	133.01	0.727

3.5.1 ANN Modeling Results

As shown in Table 8, the performance metrics show that we have an ANN model with good predictive power. The data-prediction agreement can also be seen in Figure 6, which shows both the train and the test data.

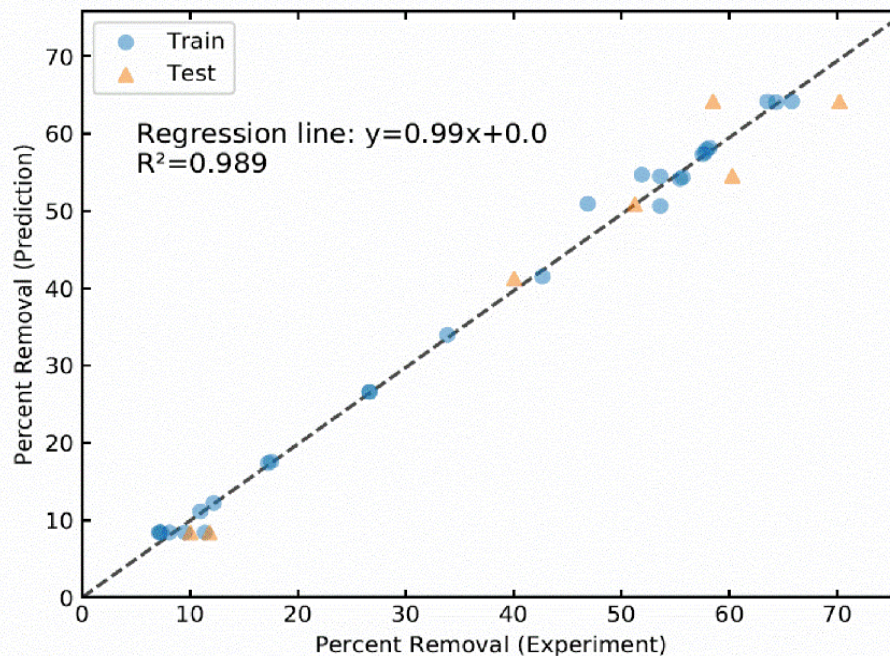


Figure 6. Data points vs. model prediction for train and test samples. The data-prediction agreement is confirmed by the regression line, which has a null intercept and close to unity slope. The coefficient of determination value shown is calculated using all available data.

We used our ANN model to do a grid search in the parameter space for the optimal reaction point. The optimal point we found was 3% initial acid concentration with 0.45g adsorbent at 45 °C temperature for 10 minutes, with the removal of 64.4%. In general, this prediction is in good agreement with both our experimental results and the RSM results shown in section 3.4. Both methods predict quite close maximum removal values. They also predict the same value for the most important independent variable, the adsorbent amount. We observe small differences in the model predictions for the remaining variables, yet none deviates significantly from neither the other model nor the experimental data. ANN models allow one to estimate the extent to which an input feature affects the model predictions. This is called the importance of a feature. We studied the relative feature importances by ranking the input features according to their relative importances as calculated using the following expression [39]:

$$I_j = \frac{\sum_{m=1}^{m=N_h} \left[\left(|W_{jm}^{ih}| / \sum_{k=1}^{N_i} |W_{km}^{ih}| \right) \times |W_{mn}^{ho}| \right]}{\sum_{l=1}^{N_i} \left\{ \sum_{m=1}^{m=N_h} \left(|W_{lm}^{ih}| / \sum_{k=1}^{N_i} |W_{km}^{ih}| \right) \times |W_{mn}^{ho}| \right\}} \quad (11)$$

which gives the relative importance of the j^{th} input feature. In this expression, N_i and N_h are the number of neurons in the input and hidden layers, respectively. W_{jm}^{ih} terms are the weights for the connection between the j^{th} (input layer) and m^{th} (hidden layer) neurons, while W_{mn}^{ho} weights are for the connections between the hidden and output layers. Note that I_j values are in the interval $[0, 1)$ and should add up to unity. Relative importance results show that the adsorbent amount is the most important feature for the model results ($I=0.52$), reaction time being the next ($I=0.20$), temperature and concentration being the least (both about $I=0.14$). These results are also consistent with the RSM results shown in section 3.4.

4. CONCLUSIONS

In this study, the removal of OxA from an aqueous solution using LDH, optimizing the conditions and determining the kinetic model and modeling with both RSM and ANN are introduced for the first time. According to the obtained results, the adsorption mechanism showed good agreement with Langmuir isotherm with monolayer homogenous adsorption mechanism. Also, the kinetic studies showed that the adsorption of OxA with LDH follows the Lagergren kinetic model. The RSM model optimum process conditions were predicted as 8.17 min, 4.63% initial acid concentration 0.45 g adsorbent at 298 K with 67.75 % OxA removal. The ANN model predicted the optimum process conditions as 10 min, 3% initial acid concentration 0.45 g adsorbent at 318 K with 64% OxA removal. Comparing both the ANN and RSM results, the values of R^2 and MSE and the model predictions exhibited that the two models yielded consistent results with reasonable accuracy. Both models show that the adsorbent amount is the most important independent variable for the % OxA removal.

REFERENCES

- [1] Skwarek E. (2015) Thermal analysis of hydroxyapatite with adsorbed oxalic acid. J Therm Anal Calorim 122: 33-45. <https://doi.org/10.1007/s10973-015-4692-z>.
- [2] Jung YH, Kim KH (2015) Acidic pretreatment, Pretreatment of Biomass, in: A. Pandey, P. Binod, S. Negi, C. Larroche (Eds), Elsevier, 27-50. <https://doi.org/10.1016/B978-0-12-800080-9.00003-7>.
- [3] Sun J, Bostick BC, Mailloux BJ, Ross JM, Chillrud SN (2016) Effect of oxalic acid treatment on sediment arsenic concentrations and lability under reducing conditions. J Hazard Mater 311: 125-133. <https://doi.org/10.1016/j.jhazmat.2016.02.060>.
- [4] Lee JW, Rodrigues RC, Jeffries TW (2009) Simultaneous saccharification and ethanol fermentation of oxalic acid pretreated corncob assessed with response surface methodology, Bioresour Technol 100:6307-6311. <https://doi.org/10.1016/j.biortech.2009.06.088>.

- [5] Abollino O, Aceto M, Malandrino M, Sarzanini C, Mentasti E (2003) Adsorption of heavy metals on Nanomontmorillonite. Effect of pH and organic substances. *Water Res* 37:1619-1627. [https://doi.org/10.1016/S0043-1354\(02\)00524-9](https://doi.org/10.1016/S0043-1354(02)00524-9).
- [6] Adamu H, Anderson JA (2015) Insights into competitive adsorption between nitrate and oxalic acid over TiO₂ and consequences for photocatalytic remediation, *Proceedings of the World Congress on New Technologies (NewTech 2015)*, Barcelona, Spain, p. 17.
- [7] Wu J, Wang J, Li H, Li Y, Du Y, Yang Y, Jia X (2017) Surface activation of MnNb₂O₆ nanosheets by oxalic acid for enhanced photocatalysis. *Appl Surf Sci* 403:314-325. <https://doi.org/10.1016/j.apsusc.2017.01.170>.
- [8] Manzak A, Inal M (2014) The 2014 World Congress on Advances in Civil, Environmental, and Materials Research (ACEM14) August, Busan, pp 24–28.
- [9] Crahan KK, Hegg D, Covert DS, Jonsson H (2004) An exploration of aqueous oxalic acid production in the coastal marine atmosphere. *Atmos Environ* 38:3757-3764. <https://doi.org/10.1016/j.atmosenv.2004.04.009>.
- [10] Oke OL (1969) Oxalic acid in plants and in nutrition. *World Rev Nutr Diet* 10:262-303. <https://doi.org/10.1159/000387569>.
- [11] Baylan N, Çehreli S (2020) Experimental and modeling study for the removal of formic acid through bulk ionic liquid membrane using response surface methodology. *Chem Eng Commun* 207:1426-1439. <https://doi.org/10.1080/00986445.2019.1656076>
- [12] Liu F, Peng C, Wilson BP, Lundström M (2019) Oxalic acid recovery from high iron oxalate waste solution by a combination of ultrasound-assisted conversion and cooling crystallization. *ACS Sustainable Chem Eng* 20:17372-17378. <https://doi.org/10.1021/acssuschemeng.9b04351>
- [13] Kirsch T, Maurer G (1996) Distribution of oxalic acid between water and organic solutions of tri-n-octylamine. *Ind Eng Chem Res* 35:1722-1735. <https://doi.org/10.1021/ie9505827>.
- [14] Uslu H, Baykal E, Gök A, Kırbaşlar Şİ, Santos D (2020) Study on Oxalic Acid Extraction by Tripropylamine: Equilibrium and Computational COSMO-SAC Analysis. *J Chem Eng Data*, 65:4347-4353. <https://doi.org/10.1021/acs.jced.9b01150>.
- [15] Hasret E, Kırbaşlar Şİ, Uslu H (2019) Comparison of extractability of oxalic acid from dilute aqueous solutions using dioctylamine and trioctylphosphine oxide. *J Chem Eng Data* 64:1275–1280. <https://doi.org/10.1021/acs.jced.8b01155>.
- [16] Sarı SK, Özmen D (2018) Design of optimum response surface experiments for the adsorption of acetic, butyric, and oxalic acids on Amberlyst A21. *J Disper Sci Technol* 39:305-309. <https://doi.org/10.1080/01932691.2017.1316208>.
- [17] Özcan Ö, İnci İ, Aşçı YS, Bayazit ŞS (2017) Oxalic acid removal from wastewater using multi-walled carbon nanotubes: Kinetic and equilibrium analysis. *J Disper Sci Technol* 38:65–69. <https://doi.org/10.1080/01932691.2016.1141688>.
- [18] Jain KK, Vishwa GP, Singh N (1979) Application of flyash instead of activated carbon for oxalic acid removal. *J Chem Technol Biotechnol* 29:36-38. <https://doi.org/10.1002/jctb.503290107>.

- [19] Singh T, Sharma V, Chandrawat U, Rani A (2005) Studies on adsorption of oxalic acid on pure activated carbon, power plant flyash and their mixed blends-A kinetic approach. *Indian Journal of Environmental Protection* 25:839-847.
- [20] Ikram M, Rehman AU, Ali S, Bakhtiar SUH, Alam S (2016) The adsorptive potential of chicken egg shells for the removal of oxalic acid from wastewater. *Journal of Biomedical Engineering and Informatics* 2:118-130. <https://doi.org/10.5430/jbei.v2n2p118>.
- [21] Preocanin T, Majic Z, Kovačević D, Kallay N (2007) Adsorption of oxalic acid onto hematite: Application of surface potential measurements. *Adsorption Science & Technology* 25:429-437. <https://doi.org/10.1260/026361707783908300>
- [22] Zhang X, Zhang L, Zou X, Han F, Yan Z, Li Z, Hu S (2018) Semi-quantitative analysis of microbial production of oxalic acid by montmorillonite sorption and ATR-IR. *Applied Clay Science* 162:518-523. <https://doi.org/10.1016/j.clay.2018.07.006>.
- [23] Xue X, Wang W, Fan H, Xu Z, Pedruzzi I, Lil P, Yu J (2019) Adsorption behavior of oxalic acid at water–feldspar interface: experiments and molecular simulation. *Adsorption* 25:1191–1204. <https://doi.org/10.1007/s10450-019-00111-8>.
- [24] Li C, Wei M, Evans DG, Duan X (2014) Layered double hydroxide-based nanomaterials as highly efficient catalysts and adsorbents. *Small* 10:4469–4486. <https://doi.org/10.1002/smll.201401464>.
- [25] Vreysen S, Maes A (2008) Adsorption mechanism of humic and fulvic acid onto Mg/Al layered double hydroxides. *Appl Clay Sci* 38:237–249. <https://doi.org/10.1016/j.clay.2007.02.010>.
- [26] Gök A, Gök MK, Aşçı YS, Lalikoğlu M (2014) Equilibrium, kinetics and thermodynamic studies for separation of malic acid on layered double hydroxide (LDH). *Fluid Ph Equilibria* 372: 15-20. <https://doi.org/10.1016/j.fluid.2014.03.023>.
- [27] Hosseini SA, Akbari M (2016) ZnO/Mg-Al Layered double hydroxides as a photocatalytic bleaching of methylene orange - A Black box modeling by artificial neural network. *Bull Chem React Eng Catal* 11:299-315. <http://doi.org/10.9767/bcrec.11.3.570.299-315>
- [28] Yasin Y, Ahmad FBH, Moghaddam MG, Khajeh M (2014) Application of a hybrid artificial neural network–genetic algorithm approach to optimize the lead ions removal from aqueous solutions using intercalated tartrate-Mg–Al layered double hydroxides. *Environ Nanotechnol Monit Manag* 2: 2-7. <https://doi.org/10.1016/j.enmm.2014.03.001>.
- [29] Kalavathy H, Regupathi MI, Pillai MG, Miranda LR (2009) Modelling, analysis and optimization of adsorption parameters for H₃PO₄ activated rubber wood sawdust using response surface methodology (RSM). *Colloids Surf B* 70:35–45. <https://doi.org/10.1016/j.colsurfb.2008.12.007>.
- [30] Bezerra MA, Santelli RE, Oliveira EP, Villar LS, Escalera LA (2008) Response surface methodology (RSM) as a tool for optimization in analytical chemistry. *Talanta*. 76:965–977. <https://doi.org/10.1016/j.talanta.2008.05.019>.

- [31] Seron A, Delorme F (2008) Synthesis of layered double hydroxides (LDHs) with varying pH: A valuable contribution to the study of Mg/Al LDH formation mechanism. *J Phys Chem Solids* 69:1088-1090. <https://doi.org/10.1016/j.jpcs.2007.10.054>.
- [32] Chao YF, Chen PC, Wang SL (2008) Adsorption of 2,4-D on Mg/Al-NO₃ layered double hydroxides with varying layer charge density. *Appl Clay Sci* 40:193-200. <https://doi.org/10.1016/j.clay.2007.09.003>
- [33] Ho Y, McKay G (1999) Pseudo-second order model for sorption processes. *Process Biochem* 34:451-465. [https://doi.org/10.1016/S0032-9592\(98\)00112-5](https://doi.org/10.1016/S0032-9592(98)00112-5).
- [34] Azizian S (2004) Kinetic models of sorption: a theoretical analysis. *J Colloid Interface Sci* 276:47-52. <https://doi.org/10.1016/j.jcis.2004.03.048>.
- [35] Aharoni C, Tompkins FC (1970) Kinetics of adsorption and desorption and the Elovich equation. *Adv Catal* 21:1-49. [https://doi.org/10.1016/S0360-0564\(08\)60563-5](https://doi.org/10.1016/S0360-0564(08)60563-5).
- [36] Foo KY, Hameed BH (2010) Insights into the modeling of adsorption isotherm systems. *Chem Eng J* 156:2-10. <https://doi.org/10.1016/j.cej.2009.09.013>.
- [37] Bashir MJK, Aziz HA, Yusoff MS, Adlan MN (2010) Application of response surface methodology (RSM) for optimization of ammoniacal nitrogen removal from semi-aerobic landfill leachate using ion exchange resin. *Desalination* 254:154-161. <https://doi.org/10.1016/j.desal.2009.12.002>.
- [38] Muhamad MH, Abdullah SRS, Mohamad AB, Rahman RA, Kadhum AAH (2013) Application of response surface methodology (RSM) for optimisation of COD, NH₃-N and 2,4-DCP removal from recycled paper wastewater in a pilot-scale granular activated carbon sequencing batch biofilm reactor (GAC-SBBR). *J Environ Manage* 121:179-190. <https://doi.org/10.1016/j.jenvman.2013.02.016>.
- [39] Garson GD (1991) Interpreting neural-network connection weights. *AI Expert* 6:47-51.